ADVANCED OPTICAL MATERIALS
www.advopticalmat.de

Recent Progress on Optoplasmonic Whispering-Gallery-Mode Microcavities

Yongpeng Chen, Yin Yin, Libo Ma,* and Oliver G. Schmidt*

Optoplasmonic whispering-gallery-mode (WGM) microcavities, consisting of plasmonic nanostructures and optical microcavities, provide excellent platforms for exploring fundamental mechanisms as well as facilitating novel optoplasmonic applications. These integrated systems support hybrid modes with both subwavelength mode confinement and high-quality factor which do not exist in either pure optical WGM microcavities or plasmonic resonators. In this progress report, geometric designs and fabrication strategies of optoplasmonic microcavities, which efficiently bridge the interaction between resonant light and plasmonic resonances, are reviewed in detail. Three types of hybrid modes in the optoplasmonic microcavities, that is, surface-plasmon-polariton whispering-gallery modes, hybrid photon–plasmon whispering-gallery modes, and heterostructured metal–dielectric whispering-gallery modes, are considered. These modes are characterized by a largely enhanced evanescent field that is referred to as a plasmon-type field in hybrid whispering-gallery modes. Moreover, the coupling effect between localized surface plasmon resonances and whispering-gallery modes is summarized. The underlying coupling mechanisms and their influence on mode shifts, *Q* factor, mode splitting, and line shapes of the whispering-gallery modes are discussed. Applications based on optoplasmonic WGM microcavities including enhanced sensing, nanolasing, and free-space coupling are highlighted, followed by an outlook of the opportunities and challenges in developing large-scale on-chip integrated optoplasmonic systems.

1. Introduction

Optical microcavities, capable of confining and manipulating light in a relatively small volume with high-quality factor, have gained considerable attention ranging from fundamentals in enhanced light-matter interactions to advanced sensing and lasing applications.[1–12] Based on the confinement mechanism, optical microcavities can be categorized into Fabry–Pérot, photonic crystal, and whispering-gallery-mode (WGM) type cavities. Among them, WGM microcavities confining light by total internal reflection can achieve high-quality resonances greatly pushing the development of cavity quantum electrodynamics, nonlinear optics, quantum optics, and non-Hermitian photonics.[13–16]

To further enhance the electric field strength in WGM cavities, plasmonic nanostructures have been introduced, which are referred to as optoplasmonic WGM microcavities.[17] Plasmonic modes, including surface plasmon polaritons or localized surface plasmon resonances (LSPRs), are well known for deep subwavelength confinement and strong near-field

Y. Chen, Dr. Y. Yin
School of Materials Science and Engineering
Jiangsu University
Zhenjiang 212013, China
E-mail: y.yin@outlook.com

Dr. Y. Yin, Dr. L. Ma, Prof. O. G. Schmidt
Institute for Integrative Nanosciences
Leibniz IFW Dresden
01069 Dresden, Germany
E-mail: y.yin@outlook.com; l.ma@ifw-dresden.de

The ORCID identification number(s) for the author(s) of this article can be found under https://doi.org/10.1002/adom.202100143.

DOI: 10.1002/adom.202100143

Prof. O. G. Schmidt
Material Systems for Nanoelectronics
Technische Universität Chemnitz
09107 Chemnitz, Germany

Prof. O. G. Schmidt
Center for Materials, Architectures and Integration of Nanomembranes (MAIN)
Technische Universität Chemnitz
09126 Chemnitz, Germany

Prof. O. G. Schmidt
Nanophysics, Faculty of Physics
Technische Universität Dresden
01062 Dresden, Germany

enhancement effects.[18–21] However, the large imaginary part of the material permittivity in noble metal media, such as Au, Ag, Cu, etc., causes large absorption losses by the plasmonic resonances. The combination of plasmonic nanostructures with dielectric WGM microcavities, on one hand, secures the sub-wavelength-scale mode volume in plasmonic modes together with the strong near-field enhancement. On the other hand, the absorption loss of metal nanostructures is compensated by the dielectric WGM microcavities which provide low-loss storage of the optical field.

Over the past decade, optoplasmonics in hybrid systems consisting of metallic nanostructures (e.g., thin films, nanorods, and nanoparticles) and WGM microcavities (e.g., microtoroid, microdisk, and microtube) have been extensively investigated.[22–26] The hybrid integration provides an excellent platform not only for exploring novel photon–plasmon modes that cannot exist in either pure WGM cavities or plasmonic nanoresonators, but also for efficiently bridging the interaction between resonant light and plasmonic resonances. In this progress report, hybrid micro- and nano-structured optoplasmonic WGM microcavities are introduced in Section 2, where geometric designs and fabrication strategies are reviewed in detail. In Sections 3–5, three types of resonant modes supported by optoplasmonic WGM microcavities are discussed, that is, surface-plasmon-polariton (SPP) WGMs, hybrid photon–plasmon (HPP) WGMs, and heterostructured metal-dielectric (HMD) WGMs. These modes are characterized by the largely enhanced evanescent field that is referred to as plasmon-type field with promising features for light-matter interactions and related applications. In Section 6, we review the coupling effect between LSPRs and WGMs, which causes mode shifts, quality factor changes, mode splittings, and line shape deformations to occur in the hybrid microcavities. In the final section, applications based on optoplasmonic WGM microcavities are highlighted, followed by an outlook and a discussion of the application potential of large-scale on-chip integrated sensors, lasers, and photonic communication components.

2. Configurations and Fabrications

2.1. WGM Microcavities

Over a hundred years ago, Lord Rayleigh introduced the term "whispering gallery" mode to describe sound waves propagating along the gallery surface of St Paul's Cathedral.[27] For the photonic counterpart, however, it took some more time until advanced micro- and nanofabrication technologies were developed. Quality (Q) factor and mode volume are two main parameters to judge the optical performance of a WGM microcavity. The Q factor is defined as the ratio of the energy stored in the oscillating cavity to the energy dissipated per cycle by damping processes, which can be expressed by $Q = \frac{\lambda_0}{\lambda_w} = \omega\tau$, where λ_0 is the central wavelength of a WGM, λ_w is its full-width-half-maximum, ω is the angular frequency, and τ is the decay time for the stored energy. In general, a higher Q factor indicates a longer photon resonating time, allowing for enhanced light-matter interactions. An optical microcavity with a Q factor ranging from 10^3 to 10^6 is considered a high-Q cavity, while that with a Q factor > 10^7 is referred to as an ultrahigh-Q cavity.[1] The mode volume describes the ability to confine the trapped light within a certain volume in the spatial domain of an optical cavity. It is defined as the ratio of the stored energy of light and the maximum energy density: $V = \frac{\int \varepsilon(\mathbf{r})|E(\mathbf{r})|^2 d^3\mathbf{r}}{\max[\varepsilon(\mathbf{r})|E(\mathbf{r})|^2]}$, where $\varepsilon(\mathbf{r})$ is the optical permittivity of the cavity material and $|E(\mathbf{r})|^2$ is the electric field. A small mode volume implies a highly localized optical field which can efficiently mediate the interaction between light and matter.

Several types of optical WGM microcavities have been exploited. According to their geometry, they can be classified as microspheres, microbottles, microdisks, microtoroids, microrings, and microtubes (**Figure 1**a). In the early stage, silica capillaries or telecom fibers were adopted to fabricate microspheres, microbottles, and microtube cavities because of the low cost and simple fabrication approach.[28–33] For instance, by melting the tip of a capillary or fiber using CO_2 laser fusion or a gas flame, surface tension forces creates cavities of spherical shape. Thanks to the extremely low optical loss enabled by smooth surfaces and low-loss materials, a Q factor as high as 10^9 was achieved.[34] In addition, the microsphere cavities can support very complicated high-order WGMs with equatorial, radial, and polar field dependence. Another trick called "heat-and-pull" has been applied to prepare microbottle cavities, which experience a diameter gradient along the cavity axis.[35,36] Resonant light oscillates along the cavity axis forming 3D WGMs with ultrahigh Q factors together with convenient wavelength tunability.[35–37]

Along with the recent development of top-down micro- and nanofabrication technologies, on-chip integrated semiconductor microcavites have been manufactured.[38–43] In 1992, S. McCall et al. exploited lithography techniques to prepare a microdisk cavity using the InP/InGaAsP system and demonstrated WGM lasing with a low threshold for the first time.[38] To further improve the Q factor, various etching methods, for example, reactive-ion-beam etching, inductively coupled plasma reaction ion etching, chemically assisted ion-beam etching, wet etching, have been developed to decrease the scattering loss induced by the imperfections on the semiconductor cavity surface.[40,43] In recent explorations, lithium-niobate-on-insulator (LNOI) microdisks have been prepared using chemo-mechanical polish lithography.[44] High-Q lasing modes were realized which hold great potential in future low-loss large-scale photonic integration for optical communications and information processing.[45,46] Furthermore, different boundary shapes of a microdisk were investigated to enhance the mode confinement in the cavity. It has been demonstrated that a wedged-shaped edge with isolated modes from the disk perimeter could largely reduce the scattering loss.[47] A microtoroid cavity, fabricated by deforming the sharp edge surface to a toroid surface with a CO_2 laser has reached an ultra-high Q factor in excess of 10^8.[48]

Microring cavities, compatible with complementary metal-oxide semiconductor (CMOS) micro-and nanofabrication technologies, have great prospects in next-generation optical communication networks and optofluidic chips.[49,50] In particular, vertical microring cavities, fabricated by rolled-up

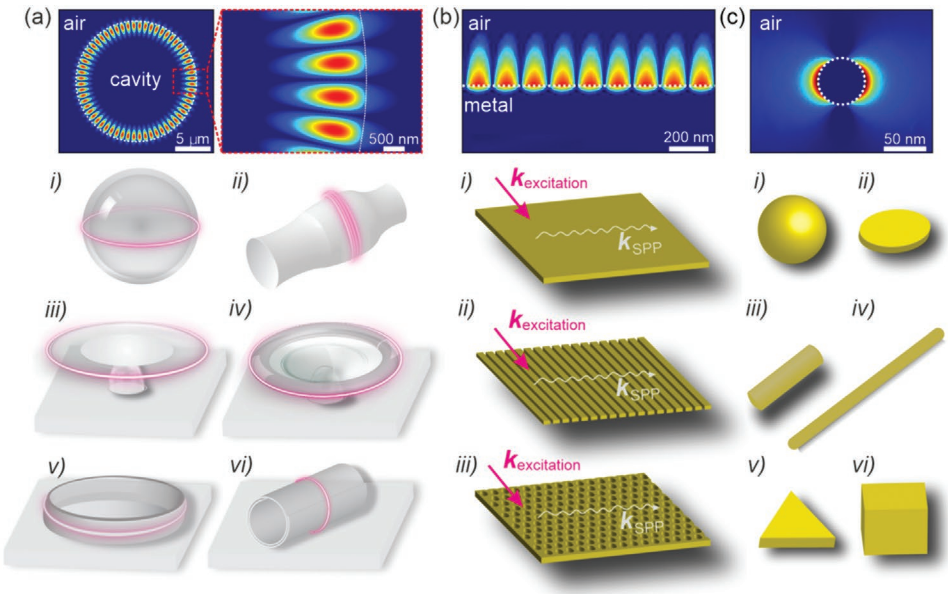

Figure 1. Optical WGM microcavities and plasmonic nanostructures. a) Representative electric field distributions of a WGM in an optical WGM microcavity. i–vi) Schematic diagrams of a microsphere, microbottle, microdisk, microtoroid, microring, and microtube cavity, respectively. b) Representative electric field distribution of SPPs at the metal-air interface. i–iii) Schematic diagrams of a metallic nanofilm, nanograting, and nanoholes, respectively. c) Representative electric field distribution of an LSPR in a metallic nanosphere. i–vi) Schematic diagrams of a metallic nanosphere, nanodisk, nanorod, nanowire, nanotriangle, and nanocube, respectively.

nanotech,[51–53] possess ultra-thin cavity walls down to 150 nm, enabling strong evanescent field coupling to on-chip waveguides, highly sensitive label-free optical sensing performance, and enhanced light-matter interactions.[26,54–64]

2.2. Plasmonic Nanostructures

For the plasmonic counterpart, rather than dielectric materials, noble metals such as Ag, Au, Cu, Al, etc., with various geometries and sizes have been investigated.[21] Surface plasmons originate from collective electron oscillations located at the interface between a metal surface and a dielectric under excitation. When using light excitation, the coupling between the incidence and surface plasmons gives rise to SPPs or LSPRs depending on the geometry of the metallic nanostructures. Due to the combination of electrons and photons, SPPs and LSPRs provide high localization and strong confinement regardless of the diffraction limit of light. However, the huge absorption loss of noble metals severely reduces the Q factors of plasmonic resonators, which are generally smaller than 100. To address this issue, great efforts have been devoted to find novel material systems and advanced synthesis techniques towards low-loss metallic nanostructures.[65–68]

SPPs, existing at continuous or periodic metal surfaces, for example, planar films, gratings, and nanohole arrays, are confined modes in the form of traveling waves with subwavelength mode volume at the metal-dielectric interface (Figure 1b). The propagation wavevector of SPPs is larger than the incident light in free space, so that momentum transfer enabled by certain coupling techniques, such as prism coupling and grating coupling, are required for the SPPs excitation. In addition, using an optical probe of the scanning near-field optical microscope as a special point source provided local excitation and propagation visualization of SPP waves.[69,70] Due to excellent field confinement, SPPs are considered as one of the most promising candidates for constructing subwavelength photonic devices, for example, interferometers, waveguides, nanolasers.[71,72]

Unlike SPPs propagating on metal-dielectric interfaces, LSPRs are strongly localized by metal nanostructures, for example, nanospheres, nanodisks, nanorods, nanowires, etc (Figure 1c). The working wavelength of LSPRs ranging from ultraviolet to near-infrared is tunable by materials as well as geometric size. For instance, aluminum is an excellent plasmonic material in the UV and blue spectral range, while silver is suitable for blue to green light and gold is used from red to near-infrared. Generally, LSPRs continuously red-shift as the size of the nanostructures increases. The fundamental mode of LSPRs is referred to as a “dipole” mode oscillation in which the strongly scattered field near the plasmonic nanostructures acts as a dipole emission. As for complex or coupled plasmonic nanostructures, hybridization models and numerical simulations have been carefully studied to solve the resonance condition.[73] Over more than three decades, LSPRs have successfully served for surface sensing, enhanced photocatalysis, and photochemistry as well as in photothermal and photovoltaic devices and plasmonic nanolasers.[74–80]

2.3. Optoplasmonic WGM Microcavities

In very recent studies, the combination of plasmonic nanostructures and photonic dielectrics has led to a good balance

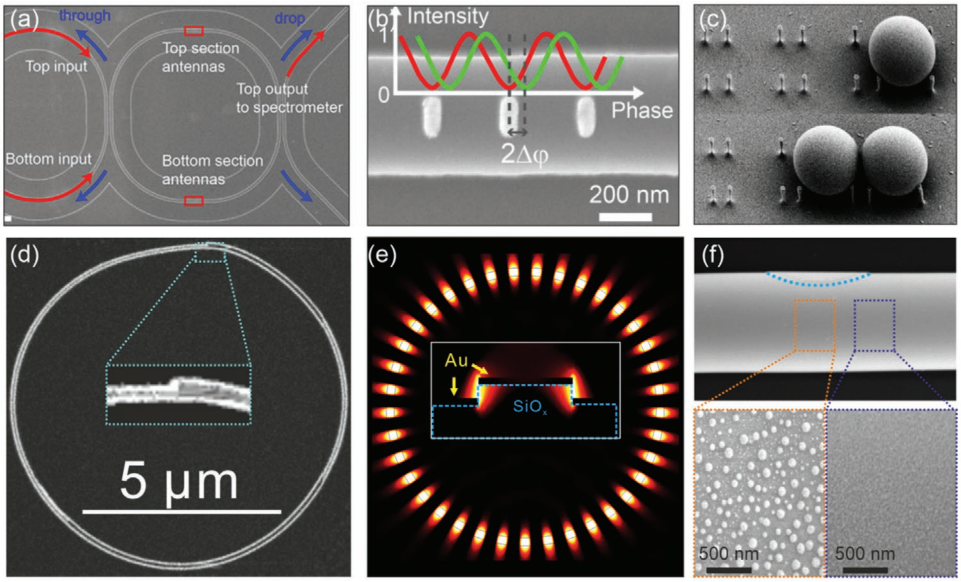

Figure 2. Integration and configuration for LSPR–WGM coupling. a) SEM image of a plasmonic-nanoantenna-integrated WGM microring cavity. b) Nanoantenna arrays located on cavity wall of a microring for the modulation of cavity WGMs. (a,b) Reproduced with permission.[90] Copyright 2018, American Chemical Society. c) SEM images of optoplasmonic WGM cavities containing microspheres and nanopillars (with gold tip). Reproduced with permission.[92] Copyright 2012, American Chemical Society. d) SEM image of the cross-section of a rolled-up microtube cavity. Inset shows a nanostep located at the edge of the rolled-up nanomembrane. e) Simulated mode profile of a WGM confined inside the ring trajectory. Inset shows the simulated intense near-field of an LSPR supported by gold nanogaps. (d,e) Reproduced with permission.[26] Copyright 2016, American Physical Society. f) SEM images of a silver-coated microtube cavity. The left bottom shows the area dewetted by a laser beam, in comparison to the right bottom without laser dewetting. Reproduced with permission.[57] Copyright 2018, American Chemical Society.

between confinement and absorption loss.[81–89] As such, enhanced light-matter interactions sit at the core of hybrid optoplasmonic systems for the development of novel nanophotonic devices for sensing, light emission, and information processing, etc.[81,83,87,89] Photonic crystals, Fabry–Pérot cavities, photonic waveguides, and optical fibers have been integrated with plasmonic nanostructures, previously.[81–83,86,88,89] However, WGM microcavities offer several significant advantages such as ultrahigh Q and fabrication simplicity, which has enabled realizations of hybrid modes and the coupling effect in optoplasmonic WGM microcavities with respect to the underlying physical mechanisms and experimental advances towards new application scenarios. By simply coating a continuous metal thin film onto the microcavity surfaces via physical vapor deposition, SPP-coupled WGM microcavities have been experimentally fabricated and investigated recently.[22] For the LSPR-coupled WGM microcavities, the size mismatch between plasmonic nanostructures and optical microcavities inevitably brings difficulties for the integration. In recent publications, tremendous efforts have been devoted to addressing this issue.

Advanced micro- and nanofabrication technologies through photolithography, electron beam lithography, dry etching, wet etching, etc., allow direct and precise integration of metal nanostructures into WGM microcavities.[90,91] Chen et al. adopted electron beam lithography and reactive ion etching to precisely pattern gold nanoantennas onto microring cavities (**Figure 2**a).[90] The controllable placement of broadband plasmonic nanoantennas onto the narrowband photonic modes leads to selective LSPR–WGM coupling. Because the radiating dipoles of plasmonic nanoantennas are in the opposite phase with the optical field of WGMs, the far-field scattering is effectively suppressed, as sketched in Figure 2b. This concept of strategically placing nanoantennas on desired positions in WGM microcavities provides ample freedom to manipulate light in complex on-chip integrated nanophotonic devices, for example, to define and select which resonances or groups of resonances are to be coupled. In addition, enhanced light-matter interactions, for example, emission enhancement from single emitters through the large cooperative Purcell effect have been demonstrated as well in a plasmonic-nanoantenna-integrated WGM microdisk cavity.[91]

Templated self-assembly combined with micro- and nanofabrication technologies provides a facile strategy to predefine WGM microcavities and plasmonic nanostructures for efficient integration.[26,92–94] Reinhard's group has developed an approach for "trapping" microsphere cavities using a template of metal-nanoparticle-tipped pillars.[92] The template was firstly introduced by standard micro- and nanofabrication technologies including electron-beam lithography, physical vapor deposition, lift-off, and reactive ion etching. In the subsequent step, the generated binding sites were filled with dielectric microsphere cavities via convective self-assembly of an aqueous solution of polystyrene spheres. Finally, the immobilization of the microsphere in the vicinity of the metal-tipped pillar completed the template-guided self-assembly, as shown in Figure 2c.

In our recent work, we have fabricated plasmonic nanogaps by depositing a gold nanofilm onto vertical nanosteps formed by spirally rolled-up microtube cavities.[26] As shown in Figure 2d, a vertical nanogap is visible from the cross-sectional image of a gold-coated microtube, which supports LSPRs with enhanced near field properties (inset of Figure 2e). The position of the plasmonic nanogaps has been conveniently tuned by depositing the gold nanofilm onto the nanosteps at different orientation angles, by which a selective coupling between axial WGMs and vertical LSPRs was realized.

Micro- and nano-manipulations implemented by a scanning probe or a glass capillary with a sharp tip are efficient to precisely place nanoobjects at a desired position. This approach has been exploited for the demonstration of metamaterial-based hyperlenses in the visible spectral range, tailored light-matter coupling in single-nanoparticle-coupled photonic crystals, and dynamic tuning of resonant modes in microtube cavities.[86,95,96] Micro- and nano-manipulations provide excellent flexibility and nondeconstructivity. In our recent work, a silver-nanoparticle-coated capillary tip (with a diameter of ≈1 μm) was mounted onto a piezo nano-manipulator to interact with the WGMs in a microtube cavity.[97] By precisely controlling the position of a plasmonic tip on a microtube cavity, competition and transition between dielectric–dielectric and plasmon–dielectric coupling were observed. In addition, the selective coupling between LSPRs supported by the capillary tip and axial optical WGMs in the microtube cavity has been achieved by shifting the tip along the tube axis.

Random assembly of plasmonic nanoparticles on WGM microcavity surfaces is a convenient and low-cost approach to create optoplasmonic cavities and study LSPR–WGM coupling.[98–106] Chemically synthesized metallic nanoparticles in solution were adsorbed on the dielectric cavity by simply drop-casting or immersing the cavity into the solution. The binding strength was set by adjusting the pH of the aqueous environment to obtain an irreversible nanoparticle adsorption process.[98] Single-plasmonic-nanoparticle-integrated WGM microcavities were produced by diluting the solution to an extremely low concentration, which has negligible absorption and scattering losses. Very recently, plasmonic enhancement causing spectral shifts of the cavity modes has improved the sensing performance of detecting single nanoparticles, viruses, proteins, nucleic acid interactions, and ions.[98,99,105–107]

Physical vapor deposition has also been applied to prepare metallic nanoparticles that are randomly assembled on WGM microcavities. For instance, aluminum, gold, and platinum nanoparticles were directly deposited on hexagonal ZnO microrod microcavities by radiofrequency magnetic sputtering.[108–111] Significant enhancement of laser intensity has been experimentally demonstrated due to charge transfer and efficient coupling between ZnO WGMs and metallic surface plasmons. The excellent stability and improved emission properties imply the great potential of this facile preparation strategy in manufacturing high-efficiency optoplasmonic devices.

Randomly distributed plasmonic nanoparticles, however, experience poor spatial controllability and accuracy. It is therefore of great importance to develop in situ fabrication protocols to place metallic nanoparticles at desired positions on an optical microcavity surface. This approach is also expected to provide better mechanical stability in a reproducible and location-selective fashion. Recently, our group has reported a laser-driven method to in situ generate plasmonic nanoparticles on silver-coated microtube cavities (Figure 2f).[57] Plasmonic nanoparticles were generated by laser annealing at a spot area of ≈ 2 μm^2 on the silver nanofilm. LSPRs supported by the nanoparticles were optimized by adjusting the silver film thickness and annealing conditions. Unlike in previous works where metallic nanoparticles were randomly distributed on the cavity surface with poor controllability, the position of silver nanoparticles in this work was precisely controlled by simply positioning the laser beam. In this way, spatially resolved coupling between LSPRs and optical WGMs could be achieved. The in situ fabrication technique provides a simple but efficient way to manipulate photon–plasmon coupling in hybrid optoplasmonic systems which are of high interest for nanophotonic tuning and enhanced light-matter interactions.

3. Surface-Plasmon-Polariton (SPP) WGMs

Due to the short propagation length of SPPs which is constrained by the large absorption in metallic materials, it is difficult to realize WGMs based on SPPs. Nevertheless, the first trial of combining dielectric microcavities with plasmonic nanostructures taken by R. Cole et al. has successfully demonstrated the evolution from traveling SPPs to confined SPP WGMs.[112] The hybrid structure was constructed by embedding dielectric microspheres into flat gold films (**Figure 3**a,b). When the encapsulation depth was small, delocalized propagation of SPPs was observed in the reflectivity spectra shown in Figure 3a where the mode energies varied with the incident angle of the excitation light. As the gold layer thickness increased, the SPPs turned into discrete nondispersive modes which were strongly confined by the individual microsphere embedded in the gold layer forming SPP WGMs (Figure 3b). However, the Q factor of SPP WGMs was lower than 100 due to large optical losses which are mainly caused by large absorption in the relatively thick metal layer as well as radiative scattering at the small-sized dielectric microspheres (with diameters of 0.4–1 μm).

Utilizing ultrahigh-Q dielectric microcavities as templates have been an efficient approach to realize high-Q SPP WGMs.[22,23,113,114] In a silver-coated silica microdisk, B. Min et al. experimentally obtained SPP WGMs with Q factors exceeding 1000.[22] The microdisk cavity with a sharp wedge structure (Figure 3c) guaranteed a remarkably low scattering loss so that Q factors up to 10^7 have been routinely achieved for pure dielectric WGMs. This type of microdisk is thus an ideal template to compensate for the absorption loss when integrating metallic structures. As shown in Figure 3c, a conformal silver layer was smoothly deposited on the microdisk surface which can support low-loss surface propagation of plasmonic modes on the beveled edge. A transmission spectrum of the SPP WGMs (Figure 3d) was measured under phase-matching conditions by a tapered fiber which was positioned underneath the beveled edge of the microdisk (sketched in the right panel of Figure 3c). To verify the mode character, a full vectorial finite-element analysis was performed, and the field distribution of an SPP WGM, as well as the dielectric mode for comparison, is shown in the inset of Figure 3d. It is notable that the mode is strongly localized at the silver–silica interface, which was therefore referred to as "internal" (IN) plasmonic WGM.

Cavity-related applications rely on the evanescent field penetrating into the outer surrounding medium. It is therefore interesting to realize "external" (EX) plasmonic WGMs located at the outmost surface of metal-coated microcavities. Y. Xiao et al. studied a silver-coated microtoroid cavity in which EX SPP

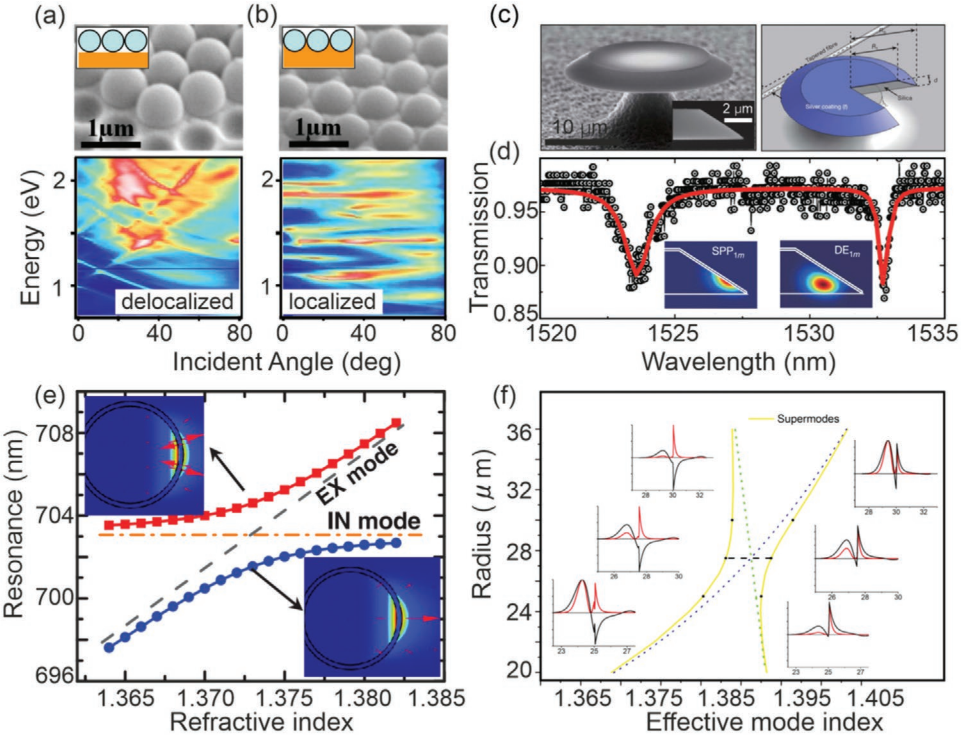

Figure 3. Investigation of SPP WGMs. a,b) Dielectric microspheres embedded into flat gold films with small depth for supporting delocalized SPP modes (a), and with large depth for supporting localized SPP WGMs (b). Reproduced with permission.[112] Copyright 2006, American Physical Society. c,d) A silver-coated microdisk cavity supporting high-*Q* SPP WGMs. Reproduced with permission.[22] Copyright 2009, Nature Publishing Group. e) Mode coupling between EX and IN SPP WGMs in a silver-coated microtoroid cavity. Reproduced with permission.[23] Copyright 2010, American Physical Society. f) Mode coupling between EX SPP WGMs and HPP WGMs in a silver-coated microsphere cavity. Reproduced with permission.[116] Copyright 2016, Optical Society of America.

WGMs were theoretically demonstrated.[23] This kind of surface mode possesses high *Q* factors at room temperature, and the calculated mode index indicated that the EX SPP WGMs could be efficiently excited by a tapered fiber under phase-matching conditions. The EX SPP WGMs exhibited a sensitivity up to 500 nm/RIU (refractive index unit) as the surrounding refraction index changed, which holds great promise for microfluidic biosensing with a large figure of merit as well as a wide detection range.

A comprehensive understanding of all types of resonant modes in metal-coated WGM microcavities is required for both fundamental studies and applications. In addition to the IN and EX SPP WGMs, HPP WGMs and dielectric (DE) WGMs originating from the transverse-magnetic (TM) and transverse-electric (TE) modes in uncoated WGM microcavities, respectively, have also been investigated.[114,115] These are discussed in detail in Section 4. It is interesting to consider the strong coupling between the different types of modes as the mode indices come close to each other, for example, IN and EX, EX and HPP, as shown in Figure 3e,f.[23,116] Eigenmode coupling in open systems is referred to as external coupling where the energy dissipation to the surrounding environment is non-negligible.[2] The resonant wavelength can be tuned by either changing the refractive index or cavity size. Strongly coupled modes, also termed supermodes, are expected to support bound states in continuum and exceptional points by modulating the external coupling strength, which offers great promise for low-threshold lasing and ultrasensitive sensing applications.[2] For microbottle or microtube cavities, the hollow core structure provides another degree of freedom for SPP WGMs.[117–120] A silver layer on the inner surface of a microbottle cavity was prepared by a silver mirror reaction occurring in the hollow core.[117,121] In such a device SPP WGMs were experimentally observed, which is of high interest for optofluidic bio-medical sensing.

4. Hybrid Photon–Plasmon (HPP) WGMs

After coating a metal layer onto optical microcavities, pure optical WGMs with TM and TE polarizations evolve into HPP and DE modes, respectively. As sketched in the top panel of **Figure 4**a, the electric field of the TM-polarized mode is perpendicular to the metal–cavity interface which matches the oscillation direction of the surface plasmons, resulting in the hybrid modes, that is, HPP modes. In contrast, the electric field of the TE-polarized mode is parallel to the metal surface (sketched in the bottom panel of Figure 4a) which results in a coupling mismatch between the cavity photons and the surface plasmons. Polarization-dependent hybrid modes have been demonstrated in metal-coated microtube cavities.[115] The hybrid structure was fabricated by directly depositing a gold nanofilm onto a silicon microtube cavity which was prepared by rolled-up nanotechnology.[51–53] This self-assembly approach has gained increasing interest in manufacturing large-scale on-chip cavity devices.[59] In fact, this kind of

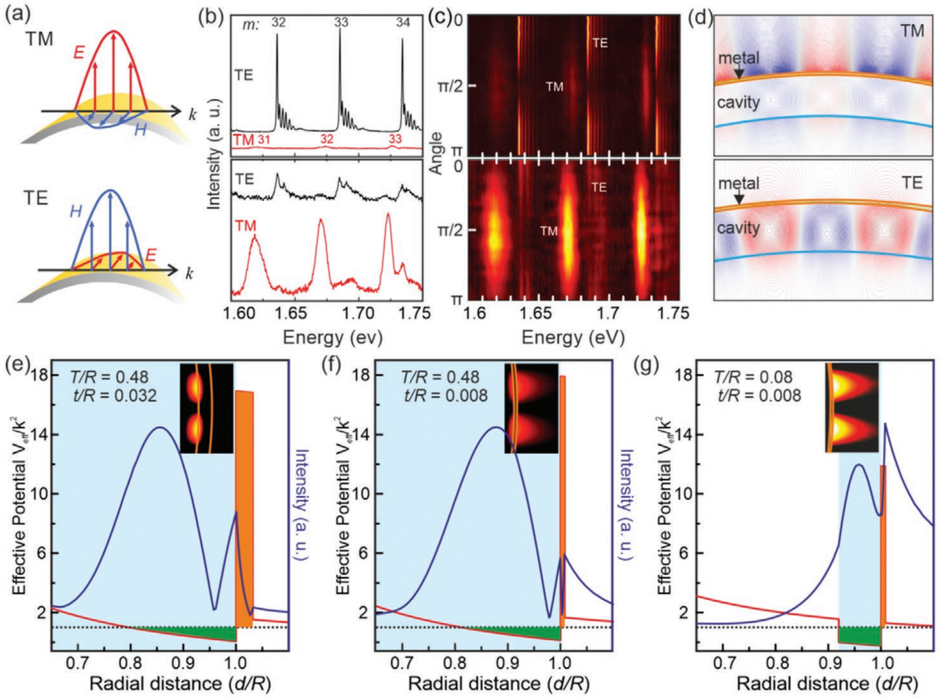

Figure 4. Investigation of HPP WGMs. a–d) Polarization dependence of the HPP WGMs in a gold-coated microtube cavity. a) Schematic diagrams of the efficient coupling between cavity photons and surface plasmons for TM-polarized modes (top) and inefficient coupling for TE-polarized modes (bottom). b) Measured spectra of both TM- and TE- polarized modes before (top) and after (bottom) metal layer coating of the WGM cavity. c) Measured polarization mappings of the same sample in (b). d) Calculated field distributions of TM- (top) and TE- (bottom) polarized modes in the gold-coated microtube cavity. Reproduced with permission.[115] Copyright 2015, American Physical Society. e–g) Three types of HPP WGMs in metal-coated microtube cavities with a varying tube wall thickness (T) and metal layer thickness (t). Field distributions and effective potentials along the radial direction of (e) weakly, (f) moderately, and (g) strongly hybridized HPP WGMs. Reproduced with permission.[125] Copyright 2016, American Physical Society.

microtube cavity has unique advantages such as ultrathin cavity walls and 3D design flexibility which has revealed new photonic phenomena like the spin-orbit coupling of resonant light.[55]

Due to the ultrathin cavity wall of microtube cavities, the evanescent field greatly extends out of the cavity surface and efficiently interacts with surface plasmons at the metal coating layer, giving rise to distinct hybrid modes. Prior to the metal layer coating, the TE-polarized modes dominate the optical resonances as its electric field is well confined within the ultrathin cavity wall (top panel of Figure 4b).[122–124] However, the TM modes become dominant as the TE modes are suppressed after coating the wall with a gold layer, as shown in the bottom panel of Figure 4b. Polarization mappings are measured for the TE and TM modes and sharp intensity contrast is visible for the situation prior to and after the gold layer coating (Figure 4c).

Electromagnetic field distributions of the TE and TM modes were calculated by the finite element method to further verify the polarization dependence of the HPP modes. Figure 4d shows the magnetic/electric field distributions along the radial direction for TM/TE modes interacting with a gold coating layer. For the TM-polarized mode, the presence of a dramatically enhanced evanescent field at the gold surface indicates a hybridization between cavity photons and surface plasmons, that is, HPP modes. Because of the polarization mismatch, the TE mode just experiences a "shielding" effect by the metal layer, which is in agreement with the mode intensity decrease observed in experiments. As there is no photon-plasmon coupling, the TE-polarized mode is referred to as dielectric mode. It is also worth mentioning that these works have clarified the favorable polarization for the excitation of HPP modes in metal-coated WGM microcavities which is of particular significance for designing hybrid optoplasmonic devices.

Based on the metal-coated microtube cavities, HPP modes with three types of plasmon-type evanescent fields have been revealed by changing the thickness of the cavity wall (T) and the metal coating layer (t).[125] For the first case, both the cavity wall and metal layer are thick, that is, T and t are comparable or larger than the wavelengths of the resonant optical light and the SPP, respectively. In this case, the plasmon-type field of the HPP mode is predominantly located at the inner surface of the metal layer, as shown in the inset of Figure 4e. Because the main field energy is stored in the photonic part of the mode in the dielectric cavity, this kind of HPP mode is referred to as weakly hybridized. When keeping T constant and decreasing t, a plasmon-type field is formed at both the inner and outer surface of the metal layer, as shown in the inset of Figure 4f. This kind of HPP mode is moderately hybridized. For the last case, T is decreased to subwavelength while t is kept constant, which is similar to the metal-coated rolled-up microtube cavities discussed above. The HPP mode in this type of optoplasmonic cavity provides an intense plasmon-type field located at the outer surface of the metal layer, as shown in the inset of Figure 4g, which is regarded as a strongly hybridized HPP mode.

An effective potential model has been used to understand the formation of these three types of HPP modes. The formation of the plasmon-type field was determined by the competition between the potential well formed by the cavity and the potential barrier induced by the metal layer.[23,113,115] The calculated potentials of the corresponding HPP modes are shown in Figure 4e–g. Cavity photons are strongly confined within the green zones of the potential wells but can also escape due to the tunneling effect. In addition, a narrower potential well means higher kinetic energy of the photons and a larger tunneling probability. The metal coating layer forms a potential barrier, the width and height of which influence the tunneling probability of the cavity photons. For the weakly hybridized HPP mode, the cavity photons confined in the potential well can hardly tunnel out of the outer boundary because: 1) the kinetic energy of the photons is low as indicated by the shallow green zone in the potential well; 2) the high and broad metal potential barrier effectively prevents the tunneling of the cavity photons. Consequently, a plasmon-type field located at the inner metal surface is generated. For the moderately hybridized HPP mode, the potential barrier was narrowed to allow the tunneling of cavity photons, which results in an additional external plasmon-type field located at the outer surface of the metal layer (Figure 4f). For the strongly hybridized HPP mode, the configuration parameters of the optoplasmonic cavity lead to the formation of a narrow potential well and low barrier (Figure 4g). In this case, the cavity photons with high kinetic energy are prone to directly tunnel out of the potential well, giving rise to the intense plasmon-type field predominantly located at the outer surface of the metal layer.

Experimental realizations of the different types of HPP modes have also been discussed in previous reports.[114–116,119] In particular, the strongly hybridized HPP mode can hardly be generated in large and thick WGM microcavities except for rolled-up microtube cavities. The microtube wall is scalable down to 100 nm, which satisfies well the hybridization requirements as discussed in the theoretical calculations. Unlike the pure SPP WGMs on the metal surface, the HPP WGMs with high Q factors are much more stable and tunable. Additionally, the intense plasmon-type field in strongly hybridized HPP modes indicates promising prospects for enhanced sensing applications.

5. Heterostructured Metal–Dielectric (HMD) WGMs

Heterostructures consisting of a metal and a dielectric offer another way to realize hybrid optoplasmonic WGM microcavities. This combination possesses the advantages of strong mode confinement and large field enhancement from the plasmonic counterpart, as well as low loss and even optical gain from the photonic counterpart.[126–131] The feasibility of heterostructure integration has been opened up by the rapidly developing synthesis techniques of low-dimensional metallic and semiconducting nanomaterials.[132–134] For instance, single silver

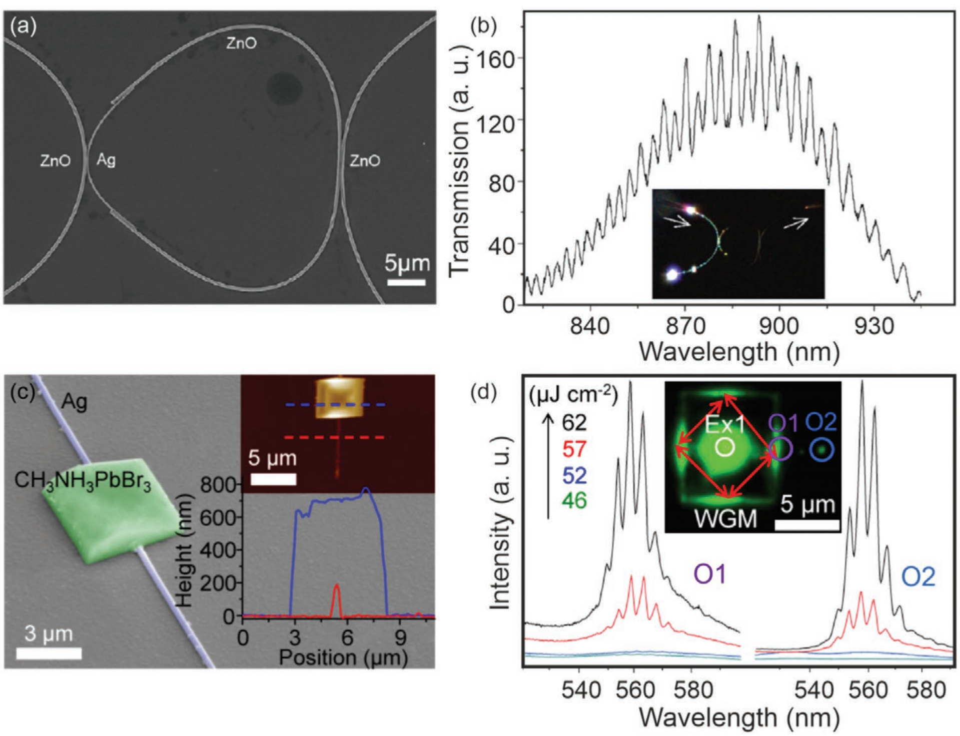

Figure 5. Fabrication and characterization of HMD WGMs. a) SEM image of ZnO–Ag nanowire heterostructures. b) Measured transmission spectrum of the hybrid rings shown in (a). Inset shows the dark field optical microscope image of the cavity under excitation. (a,b) Reproduced with permission.[136] Copyright 2009, American Chemical Society. c) SEM image of a perovskite–Ag heterostructure. Inset shows corresponding cross-section profiles of a typical heterostructure. d) Measured spectra of hybrid WGMs from the position of perovskite crystal (O1) and silver nanowire tip (O2). Inset shows the photoluminescence image of the heterostructure. (c,d) Reproduced with permission.[137] Copyright 2016, American Chemical Society.

nanowires with highly ordered crystalline structures have been chemically synthesized for the demonstration of long-range SPP propagation,[19] while for the dielectric part, single cadmium selenide nanowires with tunable bending and folding shapes have been prepared for low-threshold single-mode lasing.[135]

Micromanipulation to integrate HMD WGM microcavities with high-quality low-dimensional metals and dielectrics has been exploited in recent studies. Guo et al. prepared a metal-dielectric heterostructured WGM microcavity by connecting a silver nanowire with a zinc oxide nanowire to form a closed microring (**Figure 5**a).[136] The obtained Q factor of the hybrid cavity was up to 520, as shown in Figure 5b, which is more than five times larger than that of SPP WGMs in pure metallic microrings.[72] Although the heterostructure still had the inevitable absorption losses in the silver nanowire section, the light recirculation was greatly improved by the high coupling efficiency (up to 80%) at the metal-dielectric connections. More significantly, it provides a convenient approach to construct ultra-compact and low-attenuation nanophotonic components by decreasing the ring size and adopting high-gain semiconductor nanowires to compensate absorption losses in the metal nanowire section.

Self-assembly with controlled growth of versatile nanomaterials is an efficient way to synthesize heterostructured materials, which is also suitable for the integration of hybrid metal-dielectric WGM microcavities.[137] Recently, Li et al. prepared rationally designed metal-dielectric heterostructures consisting of a single silver nanowire embedded in a $CH_3NH_3PbBr_3$ perovskite crystal (Figure 5c) for the demonstration of a nanoscale laser via photon-plasmon coupling.[137] Due to the large curvature and high surface energies of the silver nanowires, the nucleation process of the perovskite crystal was largely facilitated. Silver nanowires were subsequently embedded by epitaxial growth of the perovskite crystals in liquid phase. As shown in Figure 5c, WGM lasing in the perovskite crystal was efficiently coupled to the plasmonic nanowires for the output emission. Laser signals collected from the dielectric edge (O1) and metallic nanowire end (O2) are shown in Figure 5d. Compared to the light spot at O1, the emission spot at O2 has a much smaller size which indicates strong confinement in the plasmonic nanowire (inset of Figure 5d). The intrinsic properties of the lasing modes from the metallic nanowire, such as the wavelength, Q factor, and polarization, are well retained, demonstrating the high-quality output via SPPs. This work provides a good inspiration for the self-assembly fabrication of heterostructured WGM microcavities to explore compact laser devices with low loss and strong confinement.

6. Coupling Effect between LSPRs and WGMs

Cavity-enhanced light-matter interactions strongly rely on small mode volume. It is therefore of high interest to further decrease the mode volume of WGMs for fundamental studies and related applications. LSPRs, supported by metal nanostructures, for example, nanospheres, nanorods, nanoantennas, etc. provide subwavelength confinement of the electromagnetic field, which can efficiently bridge the interaction between WGM microcavity and nanoobject. By now, the absorption loss from metal nanostructures is compensated by dielectric WGM microcavities with low loss or even optical gain.

In optoplasmonic microcavities, the LSPR–WGM coupling is dominated by the materials' permittivity, enhanced electric field, and absorption losses of metals. The coupling effect features distinct mode shifts and variations in Q factors of the WGMs. We have recently demonstrated uneven spectral shifts for different high-order axial modes in microtube cavities enabled by a selective coupling scheme between LSPR and WGMs.[26] When the LSPRs spatially overlap with the antinodes of certain axial WGMs, a significant mode shift occurs due to the coupling between them. On the contrary, for axial WGMs without a significant overlap between the antinodes and the LSPR, there is no mode shift due to the absence of coupling. For instance, for the metallic nanogap created in the center of the top surface of the tube, as shown in the inset of **Figure 6**a, the odd modes (i.e., E_1, E_3, E_5) exhibit a pronounced blueshift due to their efficient coupling with the LSPR. It is notable that all the modes experience blueshifts which are caused by the presence of the thin metal film. The additional mode shift of the odd modes was ascribed to the enhanced electric field of the LSPR selectively interacting with the axial WGMs.

Variations in Q factor, that is, mode broadening or narrowing, are also important to characterize the LSPR–WGM coupling, especially in a hybrid system where the mode shift is negligible.[101,138,139] As reported by Xiao's group, a dissipative interaction between single gold nanorods and a microtoroid cavity has been clearly monitored by the Q factor variation of a WGM rather than the mode shift, as shown in Figure 6c,d.[101] The coupling mechanism, on one hand, relies on the fact that the mode shift is only dependent on the real part of the polarizability of the gold nanorod. The real part of the polarizability is zero when the LSPR of the nanorod is excited. On the other hand, the Q factor variation induced by the absorption and scattering losses of the gold nanorods is significant when the WGM spectrally matches with the plasmonic resonance. Moreover, anomalous Q factor variations and mode shifts have been observed recently, which was explained by the far-field radiation interaction between the plasmonic nanostructures and the WGM microcavity.[25] Apart from the mode shift and Q factor variation, the degeneracy of clockwise (CW) and counterclockwise (CCW) WGMs has also been lifted due to symmetry breaking induced by plasmonic nanoparticles.[91] The WGM with its antinode located at the metallic nanostructure was strongly scattered while the other one remained unperturbed due to the spatial mismatch (Figure 6e,f).

As the frequency of LSPRs is far away from that of the WGMs, Fano-type resonances appear due to the coherent interaction between the spectrally broad LSPR and narrow WGMs.[102,103] Thakkar et al. presented reshapeable Fano-type WGMs via tuning a gold-nanorod-supported LSPR by thermal annealing. High-resolution spectra revealed the Fano-type WGM with different asymmetric shapes as the LSPR continuously blueshifted by increasing the heating temperature.

7. Applications and Outlook

Integration of plasmonic nanostructures into WGM microcavities gives rise to a large field enhancement and strong mode confinement which are desired in applications associated with

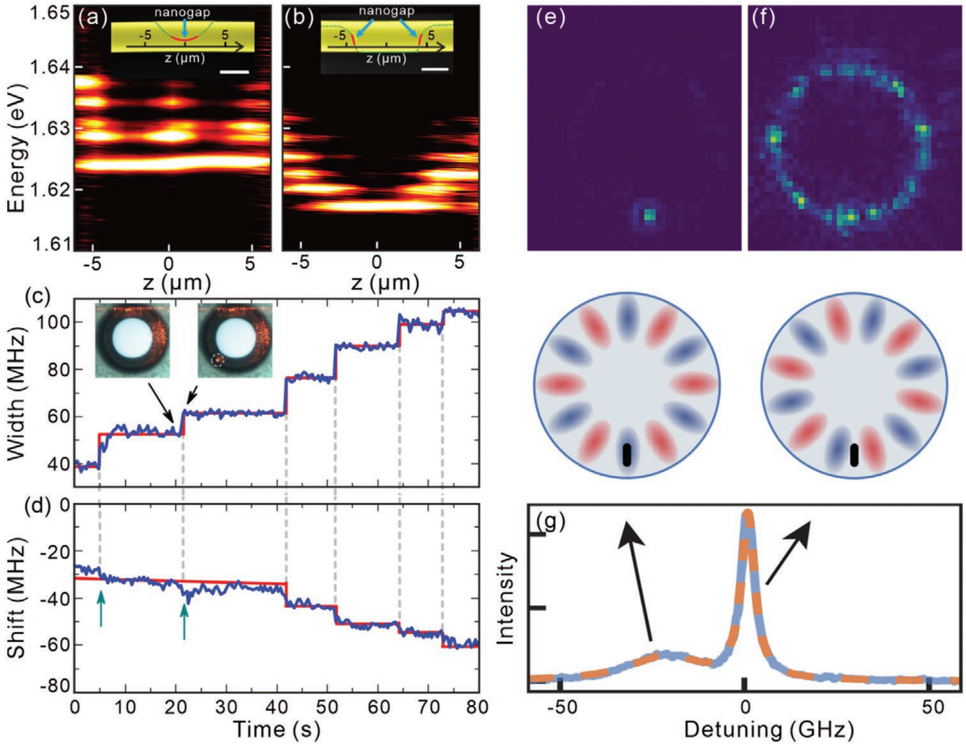

Figure 6. Mechanisms of LSPR–WGM coupling. a,b) Measured mode profile shift in plasmonic-nanogap-coupled microtube cavities with different gold nanogap locations. Reproduced with permission.[26] Copyright 2016, American Physical Society. c,d) Measured linewidth (c) and shift (d) of a WGM coupled to single gold nanorods. Reproduced with permission.[101] Copyright 2016, American Physical Society. e–g) Measured mode splitting in a plasmonic-nanoantenna-integrated microdisk cavity. Reproduced with permission.[91] Copyright 2020, American Chemical Society.

light-matter interactions. As a key application, sensing based on optoplasmonic WGMs has shown many advantages in terms of sensitivity and detection limit in recent reports.[98–100,105–107,140] The detection and analysis of single nanoparticles, molecules, proteins, viruses, and ions for physical, chemical, and biological diagnostics have been performed based on plasmonic-nanostructure-enhanced WGM microcavities. We refer the interested readers to several reviews which have discussed and summarized the optoplasmonic sensing applications in great detail.[141–146]

Plasmonic nanolasers with subwavelength mode confinement far below the diffraction limit have been considered as a promising candidate for manufacturing future ultracompact optoelectronic devices. Among the reported configurations, semiconductor WGM cavities with high optical gain and effective resonance feedback were selected to fabricate nanolaser devices by coupling with plasmonic nanostructures.[147–152] The generated lasing modes are deeply confined at either the interface or the spacer layer of the hybrid metal-dielectric structures. The strength of light-matter coupling is significantly increased due to the subwavelength mode volume of optoplasmonic WGMs. The enhancement of both spontaneous and stimulated emission rates is therefore achievable, leading to a fast response time. A higher power density is also expected for plasmonic nanolasers compared to that of conventional laser devices due to the deep field confinement. Overall, optoplasmonic WGM lasers with high radiation intensity at the nanoscale as well as fast radiation speed at the femtosecond timescale show great potential for both fundamental explorations and technological innovations.

Kwon et al. have experimentally demonstrated nanolasing with subwavelength mode volume in an optoplasmonic WGM cavity consisting of an InP disk embedded in a silver nanopan, as sketched in **Figure 7**a.[147] Lasing (Figure 7b) was clearly observed at liquid-nitrogen temperature upon optically pumping. The lasing was attributed to an SPP WGM confined at the bottom of the silver nanopan by the characteristics of the spectrum, mode profile, and polarization state. Numerical simulations further identified the character of the lasing mode, and the calculated mode volume of $0.56(\lambda/2n)^3$ which is substantially smaller than that in conventional optical cavities.[153–155] In a further study, Ma et al. reported a WGM nanolaser operating at room temperature.[149] The configuration is shown in Figure 7c consisting of a thin CdS square on top of a silver substrate separated by a 5 nm MgF_2 spacing layer. By controlling the structural geometry, single-mode lasing with a line width of about 1.1 nm was achieved (Figure 7d). In another report, nanolasing modes were precisely controlled by adjusting the shape and size of bottom metal patterns, by which both circular hybrid optoplasmonic nanolasers and uniform plasmonic nanolaser arrays have been realized.[156]

Absorption spectroscopy plays a significant role in analytical chemistry, molecular and atomic physics, biomedical detections, etc. Recently, a single-particle-absorption spectrometer was experimentally proposed based on an optoplasmonic WGM cavity.[102] As sketched in Figure 7e, a pump and probe beam

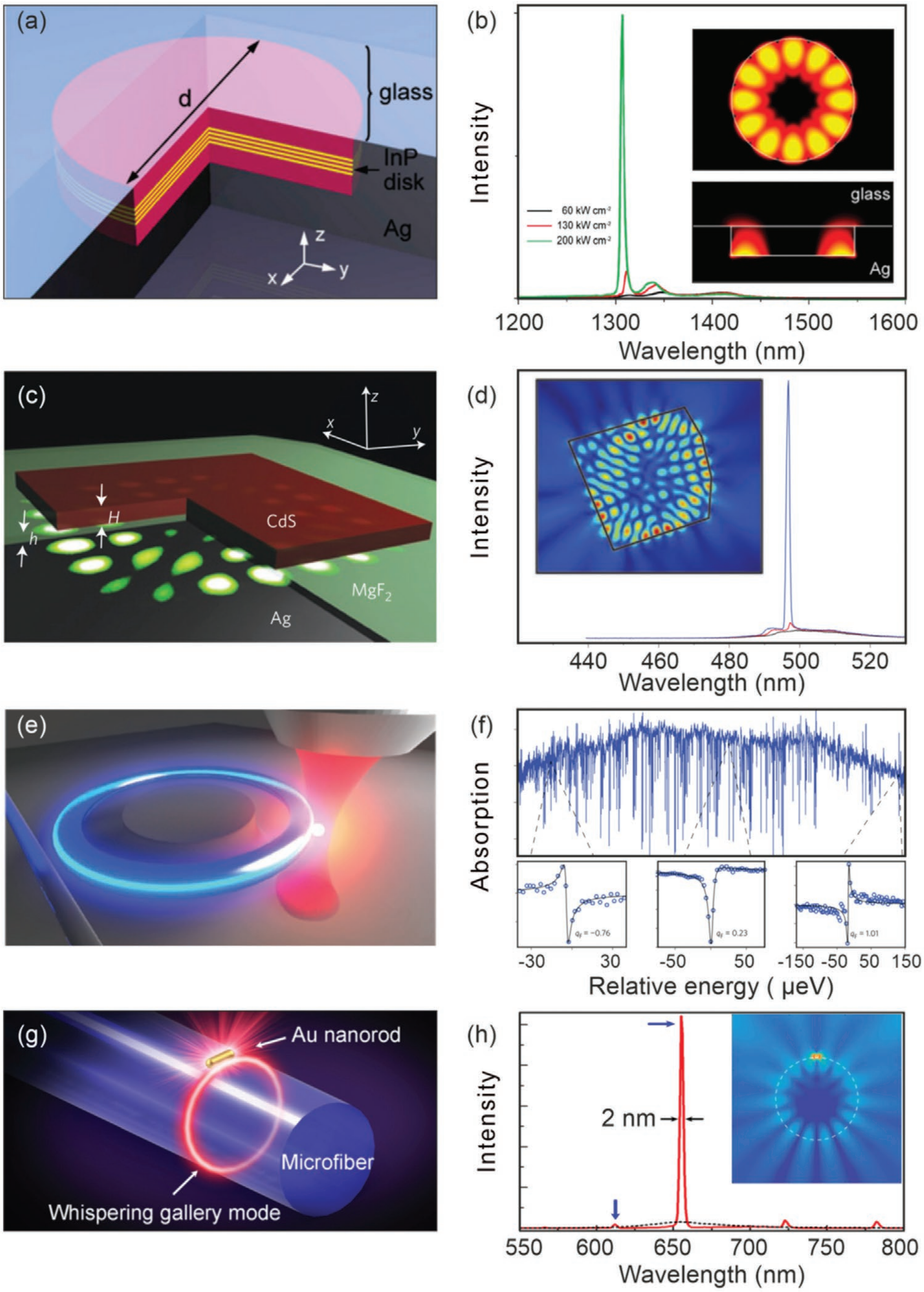

Figure 7. Applications of optoplasmonic WGM microcavities. a) Schematic diagram of a semiconductor InP disk inside a silver nanopan. b) Measured spectra of plasmonic lasing. Insets show the calculated mode profiles from the top and side view. (a,b) Reproduced with permission.[147] Copyright 2010, American Chemical Society. c) Schematic diagram of a thin CdS square on a silver substrate separated by a 5 nm MgF_2 layer. d) Measured spectra of room-temperature lasing. Inset shows the calculated field distribution of the lasing mode. (c,d) Reproduced with permission.[149] Copyright 2011, Nature Publishing Group. e) Schematic diagram of the single-nanoparticle absorption spectrometer. f) Measured spectra of asymmetric Fano-type resonances caused by coherent coupling between the LSPR and WGMs. (e,f) Reproduced with permission.[102] Copyright 2016, Nature Publishing Group. g) Schematic diagram of a gold-nanorod-integrated microfiber cavity for the realization of free-space coupling. h) Measured resonant modes from scattering spectra of a microfiber cavity with (red) and without (black dotted) single nanorod coupling. Inset shows the calculated mode profile corresponding to the experiment. (g,h) Reproduced with permission.[157] Copyright 2015, American Chemical Society.

was employed to excite a gold-nanorod-deposited high-*Q* microtoroid cavity which significantly reduced background noise. By using a parallel amplitude and phase modulation double-modulation scheme, the absorption characteristics of a single gold nanorod were monitored by high-resolution spectroscopy of asymmetric Fano resonances (Figure 7f) which were the result of the coherent coupling between the LSPR and WGMs. The hybrid system with the double-modulation technique is a sensitive platform to examine the spectral absorption information down to single molecules.

Hybrid optoplasmonic WGM microcavities have also been applied for free-space coupling. The working mechanism relies on the fact that plasmonic nanostructures are able to convert the propagation light in free space to a strongly scattered field that can enter a WGM microcavity with high efficiency. Gu and Wang et al. have independently demonstrated plasmonic-nanorod-enabled free-space coupling in silica microfiber cavities, as depicted in Figure 7g.[157,158] Interestingly, single-band emission with 30-fold enhancement in peak intensity was experimentally observed by decreasing the diameter of the microfiber (Figure 7h). This type of hybrid microcavity offers a feasible way to construct a laser device with a small mode volume and ultralow threshold. It is worth equipping these hybrid systems with more functionalities. For instance, unidirectional lasing and vortex emission has been obtained in dielectric microcavities and are also expected in optoplasmonic WGM microcavities.[159–161]

In summary, recent developments in optoplasmonic WGM microcavities have been comprehensively reviewed, including the geometric designs, fabrication strategies, fundamental mechanisms, and applications. Three types of hybrid modes, that is, SPP WGMs, HPP WGMs, and HMD WGMs, characterized by the largely enhanced evanescent field have been discussed. Integration approaches to fabricate optoplasmonic cavities as well as the underlying mechanisms to investigate the coupling effect between LSPRs and WGMs have been summarized. The hybrid systems have brought great opportunities to nanophotonic devices for sensing, lasing, absorption spectroscopy, and free-space coupling. The strong enhancement effect on light-matter interactions based on WGM microcavities may also play an important role in quantum filtering, quantum interfaces, and parity-time symmetric effects.[162,163] Further and more refined applications still require breakthroughs in reducing material losses, addressing size mismatch, and realizing large-scale on-chip integration. Once these challenges are overcome, highly integrated optoplasmonic circuits combining lasers, waveguides, filters, sensors, and spectrometers will be manufactured for applications ranging from ultra-fast information processing to physical chemistry and biomedical analysis.

Acknowledgements

This work was supported by the National Natural Science Foundation of China (Grant 11904138) and the German Research Foundation (Würzburg–Dresden Cluster of Excellence ct.qmat, EXC2147, project ID 390858490; Leibniz Program, SCHM 1298/26-1). Y.C. and Y.Y. acknowledge the support from the Natural Science Foundation of Jiangsu Province (SBK20190837), China Postdoctoral Science Foundation (2019TQ0123 and 2020M681500).

Open access funding enabled and organized by Projekt DEAL.

Conflict of Interest

The authors declare no conflict of interest.

Keywords

hybrid photon–plasmon modes, microcavities, optoplasmonic, whispering gallery modes

Received: January 21, 2021
Revised: March 1, 2021
Published online:

[1] K. J. Vahala, *Nature* **2003**, *424*, 839.
[2] H. Cao, J. Wiersig, *Rev. Mod. Phys.* **2015**, *87*, 61.
[3] S. Yang, Y. Wang, H. Sun, *Adv. Opt. Mater.* **2015**, *3*, 1136.
[4] S. Spillane, T. Kippenberg, K. Vahala, *Nature* **2002**, *415*, 621.
[5] J. McKeever, A. Boca, A. D. Boozer, J. R. Buck, H. J. Kimble, *Nature* **2003**, *425*, 268.
[6] P. Lodahl, A. F. V. Driel, I. S. Nikolaev, A. Irman, K. Overgaag, D. Vanmaekelbergh, W. L. Vos, *Nature* **2004**, *430*, 654.
[7] J. Reithmaier, G. Sęk, A. Löffler, C. Hofmann, S. Kuhn, S. Reitzenstein, L. Keldysh, V. Kulakovskii, T. Reinecke, A. Forchel, *Nature* **2004**, *432*, 197.
[8] T. Yoshie, A. Scherer, J. Hendrickson, G. Khitrova, H. Gibbs, G. Rupper, C. Ell, O. Shchekin, D. Deppe, *Nature* **2004**, *432*, 200.
[9] T. Aoki, B. Dayan, E. Wilcut, W. P. Bowen, A. S. Parkins, T. Kippenberg, K. Vahala, H. Kimble, *Nature* **2006**, *443*, 671.
[10] G. Khitrova, H. Gibbs, M. Kira, S. W. Koch, A. Scherer, *Nat. Phys.* **2006**, *2*, 81.
[11] A. M. Armani, R. P. Kulkarni, S. E. Fraser, R. C. Flagan, K. J. Vahala, *Science* **2007**, *317*, 783.
[12] J. Weiner, P.-T. Ho, *Fundamentals and Applications*, Vol. *1*, John Wiley & Sons, Hoboken, New Jersey **2008**.
[13] W. Chen, Ş. K. Özdemir, G. Zhao, J. Wiersig, L. Yang, *Nature* **2017**, *548*, 192.
[14] X. Jiang, L. Shao, S.-X. Zhang, X. Yi, J. Wiersig, L. Wang, Q. Gong, M. Lončar, L. Yang, Y.-F. Xiao, *Science* **2017**, *358*, 344.
[15] V. D. Ta, Y. Wang, H. Sun, *Adv. Opt. Mater.* **2019**, *7*, 1900057.
[16] X. Jiang, A. J. Qavi, S. H. Huang, L. Yang, *Matter* **2020**, *3*, 371.
[17] O. Benson, *Nature* **2011**, *480*, 193.
[18] S. A. Maier, *Plasmonics: Fundamentals and Applications*, Vol. *1*, Springer Science & Business Media, New York **2007**.
[19] H. Ditlbacher, A. Hohenau, D. Wagner, U. Kreibig, M. Rogers, F. Hofer, F. R. Aussenegg, J. R. Krenn, *Phys. Rev. Lett.* **2005**, *95*, 257403.
[20] J. A. Schuller, E. S. Barnard, W. Cai, Y. C. Jun, J. S. White, M. L. Brongersma, *Nat. Mater.* **2010**, *9*, 193.
[21] N. J. Halas, S. Lal, W.-S. Chang, S. Link, P. Nordlander, *Chem. Rev.* **2011**, *111*, 3913.
[22] B. Min, E. Ostby, V. Sorger, E. Ulin-Avila, L. Yang, X. Zhang, K. Vahala, *Nature* **2009**, *457*, 455.
[23] Y.-F. Xiao, C.-L. Zou, B.-B. Li, Y. Li, C.-H. Dong, Z.-F. Han, Q. Gong, *Phys. Rev. Lett.* **2010**, *105*, 153902.
[24] A. Rottler, M. Harland, M. Bröll, M. Klingbeil, J. Ehlermann, S. Mendach, *Phys. Rev. Lett.* **2013**, *111*, 253901.
[25] F. Ruesink, H. M. Doeleman, R. Hendrikx, A. F. Koenderink, E. Verhagen, *Phys. Rev. Lett.* **2015**, *115*, 203904.
[26] Y. Yin, S. Li, S. Böttner, F. Yuan, S. Giudicatti, E. S. G. Naz, L. Ma, O. G. Schmidt, *Phys. Rev. Lett.* **2016**, *116*, 253904.
[27] L. Rayleigh, *Proc. R. Soc. Lond. Ser. A* **1912**, *86*, 207.
[28] T. E. Dimmick, G. Kakarantzas, T. A. Birks, P. S. J. Russell, *Appl. Opt.* **1999**, *38*, 6845.
[29] G. Kakarantzas, T. Dimmick, T. Birks, R. L. Roux, P. S. J. Russell, *Opt. Lett.* **2001**, *26*, 1137.
[30] I. M. White, H. Oveys, X. Fan, *Opt. Lett.* **2006**, *31*, 1319.
[31] M. Sumetsky, R. Windeler, Y. Dulashko, X. Fan, *Opt. Express* **2007**, *15*, 14376.

[32] H. Zhu, I. M. White, J. D. Suter, P. S. Dale, X. Fan, *Opt. Express* **2007**, *15*, 9139.
[33] I. M. White, X. Fan, *Opt. Express* **2008**, *16*, 1020.
[34] M. L. Gorodetsky, A. A. Savchenkov, V. S. Ilchenko, *Opt. Lett.* **1996**, *21*, 453.
[35] M. Sumetsky, *Opt. Lett.* **2004**, *29*, 8.
[36] M. Sumetsky, Y. Dulashko, R. Windeler, *Opt. Lett.* **2010**, *35*, 898.
[37] M. Pöllinger, D. O'Shea, F. Warken, A. Rauschenbeutel, *Phys. Rev. Lett.* **2009**, *103*, 053901.
[38] S. McCall, A. Levi, R. Slusher, S. Pearton, R. Logan, *Appl. Phys. Lett.* **1992**, *60*, 289.
[39] R. Slusher, A. Levi, U. Mohideen, S. McCall, S. Pearton, R. Logan, *Appl. Phys. Lett.* **1993**, *63*, 1310.
[40] D. Rafizadeh, J. Zhang, S. Hagness, A. Taflove, K. Stair, S. Ho, R. Tiberio, *Opt. Lett.* **1997**, *22*, 1244.
[41] M. Fujita, K. Inoshita, T. Baba, *Electronics. Lett.* **1998**, *34*, 278.
[42] B. Gayral, J. Gérard, A. Lemaıtre, C. Dupuis, L. Manin, J. Pelouard, *Appl. Phys. Lett.* **1999**, *75*, 1908.
[43] K. Srinivasan, M. Borselli, O. Painter, A. Stintz, S. Krishna, *Opt. Express* **2006**, *14*, 1094.
[44] M. Wang, R. Wu, J. Lin, J. Zhang, Z. Fang, Z. Chai, Y. Cheng, *Quantum Eng.* **2019**, *1*, e9.
[45] Y. Liu, X. Yan, J. Wu, B. Zhu, Y. Chen, X. Chen, *Sci. China: Phys., Mech. Astron.* **2021**, *64*, 234262.
[46] Q. Luo, Z. Hao, C. Yang, R. Zhang, D. Zheng, S. Liu, H. Liu, F. Bo, Y. Kong, G. Zhang, *Sci. China: Phys., Mech. Astron.* **2021**, *64*, 234263.
[47] T. J. Kippenberg, J. Kalkman, A. Polman, K. J. Vahala, *Phys. Rev. A* **2006**, *74*, 051802.
[48] D. Armani, T. Kippenberg, S. Spillane, K. Vahala, *Nature* **2003**, *421*, 925.
[49] B. E. Little, J. Foresi, G. Steinmeyer, E. Thoen, S. Chu, H. Haus, E. Ippen, L. Kimerling, W. Greene, *IEEE Photon. Technol. Lett.* **1998**, *10*, 549.
[50] P. Rabiei, W. H. Steier, C. Zhang, L. R. Dalton, *J. Lightwave Technol.* **2002**, *20*, 1968.
[51] O. G. Schmidt, K. Eberl, *Nature* **2001**, *410*, 168.
[52] Y. Mei, G. Huang, A. A. Solovev, E. B. Ureña, I. Mönch, F. Ding, T. Reindl, R. K. Fu, P. K. Chu, O. G. Schmidt, *Adv. Mater.* **2008**, *20*, 4085.
[53] T. Kipp, H. Welsch, C. Strelow, C. Heyn, D. Heitmann, *Phys. Rev. Lett.* **2006**, *96*, 077403.
[54] L. Ma, S. Li, V. A. B. Quiñones, L. Yang, W. Xi, M. Jorgensen, S. Baunack, Y. Mei, S. Kiravittaya, O. G. Schmidt, *Adv. Mater.* **2013**, *25*, 2357.
[55] L. Ma, S. Li, V. M. Fomin, M. Hentschel, J. B. Götte, Y. Yin, M. Jorgensen, O. G. Schmidt, *Nat. Comm.* **2016**, *7*, 10983.
[56] J. Wang, Y. Yin, Q. Hao, Y.-D. Yang, S. Valligatla, E. S. G. Naz, Y. Li, C. N. Saggau, L. Ma, O. G. Schmidt, *Nano Lett.* **2018**, *18*, 7261.
[57] Y. Yin, J. Wang, X. Lu, Q. Hao, E. S. G. Naz, C. Cheng, L. Ma, O. G. Schmidt, *ACS Nano* **2018**, *12*, 3726.
[58] Y. Yin, J. Wang, X. Wang, S. Li, M. R. Jorgensen, J. Ren, S. Meng, L. Ma, O. G. Schmidt, *Sci. Adv.* **2019**, *5*, eaax6973.
[59] C. N. Saggau, F. Gabler, D. D. Karnaushenko, D. Karnaushenko, L. Ma, O. G. Schmidt, *Adv. Mater.* **2020**, *32*, 2003252.
[60] M. Dastjerdi, M. Djavid, Z. Mi, *Appl. Phys. Lett.* **2015**, *106*, 021114.
[61] X. Lin, Y. Fang, L. Zhu, J. Zhang, G. Huang, J. Wang, Y. Mei, *Adv. Opt. Mater.* **2016**, *4*, 936.
[62] H. Wang, H. Zhen, S. Li, Y. Jing, G. Huang, Y. Mei, W. Lu, *Sci. Adv.* **2016**, *2*, e1600027.
[63] Z. Tian, S. Li, S. Kiravittaya, B. Xu, S. Tang, H. Zhen, W. Lu, Y. Mei, *Nano Lett.* **2018**, *18*, 8035.
[64] J. Wang, Y. Yin, Q. Hao, Y. Zhang, L. Ma, O. G. Schmidt, *Adv. Opt. Mater.* **2018**, *6*, 1700842.
[65] P. R. West, S. Ishii, G. V. Naik, N. K. Emani, V. M. Shalaev, A. Boltasseva, *Laser Photonics Rev.* **2010**, *4*, 795.
[66] N. Jiang, X. Zhuo, J. Wang, *Chem. Rev.* **2017**, *118*, 3054.
[67] M. I. Stockman, K. Kneipp, S. I. Bozhevolnyi, S. Saha, A. Dutta, J. Ndukaife, N. Kinsey, H. Reddy, U. Guler, V. M. Shalaev, *J. Opt.* **2018**, *20*, 043001.
[68] G. V. Naik, V. M. Shalaev, A. Boltasseva, *Adv. Mater.* **2013**, *25*, 3264.
[69] B. Hecht, H. Bielefeldt, L. Novotny, Y. Inouye, D. Pohl, *Phys. Rev. Lett.* **1996**, *77*, 1889.
[70] S. I. Bozhevolnyi, V. S. Volkov, E. Devaux, T. W. Ebbesen, *Phys. Rev. Lett.* **2005**, *95*, 046802.
[71] W. L. Barnes, A. Dereux, T. W. Ebbesen, *Nature* **2003**, *424*, 824.
[72] S. I. Bozhevolnyi, V. S. Volkov, E. Devaux, J.-Y. Laluet, T. W. Ebbesen, *Nature* **2006**, *440*, 508.
[73] E. Prodan, C. Radloff, N. J. Halas, P. Nordlander, *Science* **2003**, *302*, 419.
[74] M. L. Brongersma, N. J. Halas, P. Nordlander, *Nat. Nanotechnol.* **2015**, *10*, 25.
[75] H. A. Atwater, A. Polman, *Nat. Mater.* **2010**, *9*, 205.
[76] X. Zhang, Y. L. Chen, R.-S. Liu, D. P. Tsai, *Rep. Prog. Phys.* **2013**, *76*, 046401.
[77] S. Linic, U. Aslam, C. Boerigter, M. Morabito, *Nat. Mater.* **2015**, *14*, 567.
[78] G. Baffou, R. Quidant, *Chem. Soc. Rev.* **2014**, *43*, 3898.
[79] D. J. Bergman, M. I. Stockman, *Phys. Rev. Lett.* **2003**, *90*, 027402.
[80] D. Xu, X. Xiong, L. Wu, X.-F. Ren, C. E. Png, G.-C. Guo, Q. Gong, Y.-F. Xiao, *Adv. Opt. Photonics* **2018**, *10*, 703.
[81] J. K. Hyun, T. Kang, H. Baek, D.-S. Kim, G.-C. Yi, *Nano Lett.* **2015**, *15*, 5938.
[82] A. Bisht, J. Cuadra, M. Wersäll, A. Canales, T. J. Antosiewicz, T. Shegai, *Nano Lett.* **2018**, *19*, 189.
[83] M. A. Schmidt, D. Y. Lei, L. Wondraczek, V. Nazabal, S. A. Maier, *Nat. Comm.* **2012**, *3*, 1108.
[84] D. G. Baranov, B. Munkhbat, E. Zhukova, A. Bisht, A. Canales, B. Rousseaux, G. Johansson, T. J. Antosiewicz, T. Shegai, *Nat. Comm.* **2020**, *11*, 2715.
[85] S. Götzinger, L. de S. Menezes, A. Mazzei, S. Kühn, V. Sandoghdar, O. Benson, *Nano Lett.* **2006**, *6*, 1151.
[86] M. Barth, S. Schietinger, S. Fischer, J. Becker, N. Nusse, T. Aichele, B. Lochel, C. Sonnichsen, O. Benson, *Nano Lett.* **2010**, *10*, 891.
[87] R. Ameling, L. Langguth, M. Hentschel, M. Mesch, P. V. Braun, H. Giessen, *Appl. Phys. Lett.* **2010**, *97*, 253116.
[88] R. Ameling, H. Giessen, *Nano Lett.* **2010**, *10*, 4394.
[89] P. Peng, Y.-C. Liu, D. Xu, Q.-T. Cao, G. Lu, Q. Gong, Y.-F. Xiao, *Phys. Rev. Lett.* **2017**, *119*, 233901.
[90] B. Chen, R. Bruck, D. Traviss, A. Z. Khokhar, S. Reynolds, D. J. Thomson, G. Z. Mashanovich, G. T. Reed, O. L. Muskens, *Nano Lett.* **2018**, *18*, 610.
[91] H. M. Doeleman, C. D. Dieleman, C. Mennes, B. Ehrler, A. F. Koenderink, *ACS Nano* **2020**, *14*, 12027.
[92] W. Ahn, S. V. Boriskina, Y. Hong, B. R. M. Reinhard, *ACS Nano* **2012**, *6*, 951.
[93] W. Ahn, Y. Hong, S. V. Boriskina, B. R. M. Reinhard, *ACS Nano* **2013**, *7*, 4470.
[94] Y. Hong, W. Ahn, S. V. Boriskina, X. Zhao, B. R. M. Reinhard, *J. Phys. Chem. C* **2015**, *6*, 2056.
[95] S. Schwaiger, M. Bröll, A. Krohn, A. Stemmann, C. Heyn, Y. Stark, D. Stickler, D. Heitmann, S. Mendach, *Phys. Rev. Lett.* **2009**, *102*, 163903.
[96] S. Li, L. Ma, H. Zhen, M. R. Jorgensen, S. Kiravittaya, O. G. Schmidt, *Appl. Phys. Lett.* **2012**, *101*, 231106.
[97] E. S. G. Naz, Y. Yin, J. Wang, A. Madani, L. Ma, O. G. Schmidt, *Opt. Lett.* **2020**, *45*, 5720.
[98] M. D. Baaske, M. R. Foreman, F. Vollmer, *Nat. Nanotechnol.* **2014**, *9*, 933.
[99] M. D. Baaske, F. Vollmer, *Nat. Photon.* **2016**, *10*, 733.
[100] E. Kim, M. D. Baaske, I. Schuldes, P. S. Wilsch, F. Vollmer, *Sci. Adv.* **2017**, *3*, e1603044.

[101] B.-Q. Shen, X.-C. Yu, Y. Zhi, L. Wang, D. Kim, Q. Gong, Y.-F. Xiao, *Phys. Rev. Appl.* **2016**, *5*, 024011.
[102] K. D. Heylman, N. Thakkar, E. H. Horak, S. C. Quillin, C. Cherqui, K. A. Knapper, D. J. Masiello, R. H. Goldsmith, *Nat. Photon.* **2016**, *10*, 788.
[103] N. Thakkar, M. T. Rea, K. C. Smith, K. D. Heylman, S. C. Quillin, K. A. Knapper, E. H. Horak, D. J. Masiello, R. H. Goldsmith, *Nano Lett.* **2017**, *17*, 6927.
[104] L. T. Hogan, E. H. Horak, J. M. Ward, K. A. Knapper, S. l. Nic Chormaic, R. H. Goldsmith, *ACS Nano* **2019**, *13*, 12743.
[105] V. Dantham, S. Holler, V. Kolchenko, Z. Wan, S. Arnold, *Appl. Phys. Lett.* **2012**, *101*, 043704.
[106] V. R. Dantham, S. Holler, C. Barbre, D. Keng, V. Kolchenko, S. Arnold, *Nano Lett.* **2013**, *13*, 3347.
[107] S. Shopova, R. Rajmangal, S. Holler, S. Arnold, *Appl. Phys. Lett.* **2011**, *98*, 243104.
[108] J. Lu, C. Xu, J. Dai, J. Li, Y. Wang, Y. Lin, P. Li, *ACS Photonics* **2015**, *2*, 73.
[109] Q. Zhu, F. Qin, J. Lu, Z. Zhu, H. Nan, Z. Shi, Z. Ni, C. Xu, *Nano Res.* **2017**, *10*, 1996.
[110] Y. Wang, F. Qin, J. Lu, J. Li, Z. Zhu, Q. Zhu, Y. Zhu, Z. Shi, C. Xu, *Nano Res.* **2017**, *10*, 3447.
[111] C. Xu, F. Qin, Q. Zhu, J. Lu, Y. Wang, J. Li, Y. Lin, Q. Cui, Z. Shi, A. G. Manohari, *Nano Res.* **2018**, *11*, 3050.
[112] R. Cole, Y. Sugawara, J. Baumberg, S. Mahajan, M. Abdelsalam, P. Bartlett, *Phys. Rev. Lett.* **2006**, *97*, 137401.
[113] Y.-L. Chen, C.-L. Zou, Y.-W. Hu, Q. Gong, *Phys. Rev. A* **2013**, *87*, 023824.
[114] C. Klusmann, J. Oppermann, P. Forster, C. Rockstuhl, H. Kalt, *ACS Photonics* **2018**, *5*, 2365.
[115] Y. Yin, S. Li, S. Giudicatti, C. Jiang, L. Ma, O. Schmidt, *Phys. Rev. B* **2015**, *92*, 241403.
[116] S. Cai, Y. Xiang, Y. Miao, M. Li, Y. Peng, Y. Song, *Opt. Express* **2016**, *24*, 13832.
[117] Q. Lu, M. Li, J. Liao, S. Liu, X. Wu, L. Liu, L. Xu, *Opt. Lett.* **2015**, *40*, 5842.
[118] Q. Lu, X. Chen, X. Liu, J. Guo, S. Xie, X. Wu, C.-L. Zou, C.-H. Dong, *Appl. Phys. Lett.* **2020**, *117*, 161101.
[119] J. Gu, Z. Zhang, M. Li, Y. Song, *Phys. Rev. A* **2014**, *90*, 013816.
[120] Y. Xiang, Y. Song, *IEEE Photon. J.* **2018**, *10*, 1.
[121] B.-H. Liu, Y.-X. Jiang, X.-S. Zhu, X.-L. Tang, Y.-W. Shi, *Opt. Express* **2013**, *21*, 32349.
[122] V. A. B. Quiñones, G. Huang, J. D. Plumhof, S. Kiravittaya, A. Rastelli, Y. Mei, O. G. Schmidt, *Opt. Lett.* **2009**, *34*, 2345.
[123] L. Ma, S. Kiravittaya, V. A. Bolaños Quiñones, S. Li, Y. Mei, O. G. Schmidt, *Opt. Lett.* **2011**, *36*, 3840.
[124] J. Trommer, S. Böttner, S. Li, S. Kiravittaya, M. R. Jorgensen, O. G. Schmidt, *Opt. Lett.* **2014**, *39*, 6335.
[125] Y. Yin, S. Li, V. Engemaier, S. Giudicatti, E. Saei Ghareh Naz, L. Ma, O. G. Schmidt, *Phys. Rev. A* **2016**, *94*, 013832.
[126] Y. Yan, C. Zhang, J. Y. Zheng, J. Yao, Y. S. Zhao, *Adv. Mater.* **2012**, *24*, 5681.
[127] Y. J. Li, Y. Yan, C. Zhang, Y. S. Zhao, J. Yao, *Adv. Mater.* **2013**, *25*, 2784.
[128] Y. J. Li, X. Xiong, C. L. Zou, X. F. Ren, Y. S. Zhao, *Small* **2015**, *11*, 3728.
[129] C. Wei, Y. S. Zhao, *ACS Appl. Mater. Interfaces* **2016**, *8*, 3703.
[130] Y. J. Li, Y. Hong, Q. Peng, J. Yao, Y. S. Zhao, *ACS Nano* **2017**, *11*, 10106.
[131] S. Kim, R. Yan, *J. Mater. Chem. C* **2018**, *6*, 11795.
[132] R. Yan, P. Pausauskie, J. Huang, P. Yang, *Proc. Natl. Acad. Sci. USA* **2009**, *106*, 21045.
[133] L. N. Quan, J. Kang, C.-Z. Ning, P. Yang, *Chem. Rev.* **2019**, *119*, 9153.
[134] X. Guo, Y. Ma, Y. Wang, L. Tong, *Laser Photonics Rev.* **2013**, *7*, 855.
[135] Y. Xiao, C. Meng, P. Wang, Y. Ye, H. Yu, S. Wang, F. Gu, L. Dai, L. Tong, *Nano Lett.* **2011**, *11*, 1122.
[136] X. Guo, M. Qiu, J. Bao, B. J. Wiley, Q. Yang, X. Zhang, Y. Ma, H. Yu, L. Tong, *Nano Lett.* **2009**, *9*, 4515.
[137] Y. J. Li, Y. Lv, C.-L. Zou, W. Zhang, J. Yao, Y. S. Zhao, *J. Am. Chem. Soc.* **2016**, *138*, 2122.
[138] Y.-F. Xiao, Y.-C. Liu, B.-B. Li, Y.-L. Chen, Y. Li, Q. Gong, *Phys. Rev. A* **2012**, *85*, 031805.
[139] Y. Hu, L. Shao, S. Arnold, Y.-C. Liu, C.-Y. Ma, Y.-F. Xiao, *Phys. Rev. A* **2014**, *90*, 043847.
[140] Y. Yin, J. Pang, J. Wang, X. Lu, Q. Hao, E. Saei Ghareh Naz, X. Zhou, L. Ma, O. G. Schmidt, *ACS Appl. Mater. Interfaces* **2019**, *11*, 15891.
[141] M. R. Foreman, J. D. Swaim, F. Vollmer, *Adv. Opt. Photonics* **2015**, *7*, 168.
[142] K. D. Heylman, K. A. Knapper, E. H. Horak, M. T. Rea, S. K. Vanga, R. H. Goldsmith, *Adv. Mater.* **2017**, *29*, 1700037.
[143] Y. Zhi, X. C. Yu, Q. Gong, L. Yang, Y. F. Xiao, *Adv. Mater.* **2017**, *29*, 1604920.
[144] A. Bozzola, S. Perotto, F. De Angelis, *Analyst* **2017**, *142*, 883.
[145] J. Xavier, S. Vincent, F. Meder, F. Vollmer, *Nanophotonics* **2018**, *7*, 1.
[146] S. Subramanian, H. Y. Wu, T. Constant, J. Xavier, F. Vollmer, *Adv. Mater.* **2018**, *30*, 1801246.
[147] S.-H. Kwon, J.-H. Kang, C. Seassal, S.-K. Kim, P. Regreny, Y.-H. Lee, C. M. Lieber, H.-G. Park, *Nano Lett.* **2010**, *10*, 3679.
[148] C.-Y. Wu, C.-T. Kuo, C.-Y. Wang, C.-L. He, M.-H. Lin, H. Ahn, S. Gwo, *Nano Lett.* **2011**, *11*, 4256.
[149] R.-M. Ma, R. F. Oulton, V. J. Sorger, G. Bartal, X. Zhang, *Nat. Mater.* **2011**, *10*, 110.
[150] R.-M. Ma, S. Ota, Y. Li, S. Yang, X. Zhang, *Nat. Nanotechnol.* **2014**, *9*, 600.
[151] R. M. Ma, R. F. Oulton, V. J. Sorger, X. Zhang, *Laser Photonics Rev.* **2013**, *7*, 1.
[152] M. T. Hill, M. C. Gather, *Nat. Photon.* **2014**, *8*, 908.
[153] M. H. Huang, S. Mao, H. Feick, H. Yan, Y. Wu, H. Kind, E. Weber, R. Russo, P. Yang, *Science* **2001**, *292*, 1897.
[154] X. Duan, Y. Huang, R. Agarwal, C. M. Lieber, *Nature* **2003**, *421*, 241.
[155] H.-G. Park, S.-H. Kim, S.-H. Kwon, Y.-G. Ju, J.-K. Yang, J.-H. Baek, S.-B. Kim, Y.-H. Lee, *Science* **2004**, *305*, 1444.
[156] C. Huang, W. Sun, Y. Fan, Y. Wang, Y. Gao, N. Zhang, K. Wang, S. Liu, S. Wang, S. Xiao, S. Qinghai, *ACS Nano* **2018**, *12*, 3865.
[157] P. Wang, Y. Wang, Z. Yang, X. Guo, X. Lin, X.-C. Yu, Y.-F. Xiao, W. Fang, L. Zhang, G. Lu, *Nano Lett.* **2015**, *15*, 7581.
[158] F. Gu, L. Zhang, Y. Zhu, H. Zeng, *Laser Photonics Rev.* **2015**, *9*, 682.
[159] C. Huang, C. Zhang, S. Xiao, Y. Wang, Y. Fan, Y. Liu, N. Zhang, G. Qu, H. Ji, J. Han, L. Ge, K. Yuri, Q. Song, *Science* **2020**, *367*, 1018.
[160] Y. Yin, Y. Chen, E. S. G. Naz, X. Lu, S. Li, V. Engemaier, L. Ma, O. G. Schmidt, *ACS Photonics* **2017**, *4*, 736.
[161] K. G. Cognée, H. M. Doeleman, P. Lalanne, A. F. Koenderink, *ACS Photonics* **2020**, *7*, 3049.
[162] C. Valagiannopoulos, *Quantum Eng.* **2020**, *2*, e52.
[163] B. Peng, Ş. K. Özdemir, F. Lei, F. Monifi, M. Gianfreda, G. L. Long, S. Fan, F. Nori, C. M. Bender, L. Yang, *Nat. Phys.* **2014**, *10*, 394.

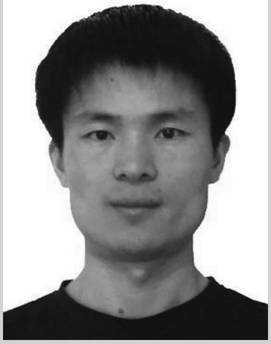

Libo Ma is a research group leader in the Institute of Integrative Nanosciences, Leibniz IFW Dresden, Germany. He received his B.S. degree in physics from Shandong Normal University, China in 2001. He obtained his Ph.D. degree from the Institute of Physics, Chinese Academy of Sciences in 2007. His current research interests include cavity photonics, plasmonics, light-matter interactions, on-chip photonic integration, and topological photonics.

Oliver G. Schmidt is the director of the Institute of Integrative Nanosciences, Leibniz IFW Dresden. He holds a full professorship for Materials Systems for Nanoelectronics at Chemnitz University of Technology, Germany. His interdisciplinary activities bridge across several research fields, ranging from nanophotonics and nanoelectronics to materials design and system engineering. His special interest lies with nanomembrane materials which can be strain-engineered and employed in multifunctional devices both on and off the chip.